Universal Method for Protein Immobilization on Chemically Functionalized Germanium Investigated by ATR-FTIR Difference Spectroscopy

ARTICLE *in* JOURNAL OF THE AMERICAN CHEMICAL SOCIETY · MARCH 2013

Impact Factor: 12.11 · DOI: 10.1021/ja400253p · Source: PubMed

7 AUTHORS, INCLUDING:

Jonas Schartner
Ruhr-Universität Bochum
10 PUBLICATIONS **24** CITATIONS
SEE PROFILE

Jörn Güldenhaupt
Ruhr-Universität Bochum
12 PUBLICATIONS **113** CITATIONS
SEE PROFILE

Bastian Mei
Technical University of Denmark
30 PUBLICATIONS **242** CITATIONS
SEE PROFILE

JACS
JOURNAL OF THE AMERICAN CHEMICAL SOCIETY

Article

pubs.acs.org/JACS

Universal Method for Protein Immobilization on Chemically Functionalized Germanium Investigated by ATR-FTIR Difference Spectroscopy

Jonas Schartner,[†] Jörn Güldenhaupt,[†] Bastian Mei,[§] Matthias Rögner,[‡] Martin Muhler,[§] Klaus Gerwert,[†] and Carsten Kötting*[,†]

[†]Department of Biophysics and [‡]Department of Plant Biochemistry, Faculty of Biology and Biotechnology, and [§]Laboratory of Industrial Chemistry, Faculty of Chemistry and Biochemistry, Ruhr-University Bochum, Germany

Supporting Information

ABSTRACT: Attenuated total reflection Fourier transform infrared (ATR-FTIR) spectroscopy allows a detailed analysis of surface attached molecules, including their secondary structure, orientation, and interaction with small molecules in the case of proteins. Here, we present a universal immobilization technique on germanium for all oligo-histidine-tagged proteins. For this purpose, new triethoxysilane derivates were developed: we synthesized a linker−silane with a succinimidyl ester as amine-reactive headgroup and a matrix−silane with an unreactive ethylene glycol group. A new methodology for the attachment of triethoxysilanes on germanium was established, and the surface was characterized by ATR-FTIR and X-ray photoelectron spectroscopy. In the next step, the succinimidyl ester was reacted with aminonitrilotriacetic acid. Subsequently, Ni^{2+} was coordinated to form Ni−nitrilotriacetic acid for His-tag binding. The capability of the functionalized surface was demonstrated by experiments using the small GTPase Ras and photosystem I (PS I). The native binding of the proteins was proven by difference spectroscopy, which probes protein function. The function of Ras as molecular switch was demonstrated by a beryllium trifluoride anion titration assay, which allows observation of the "on" and "off" switching of Ras at atomic resolution. Furthermore, the activity of immobilized PS I was proven by light-induced difference spectroscopy. Subsequent treatment with imidazole removes attached proteins, enabling repeated binding. This universal technique allows specific attachment of His-tagged proteins and a detailed study of their function at the atomic level using FTIR difference spectroscopy.

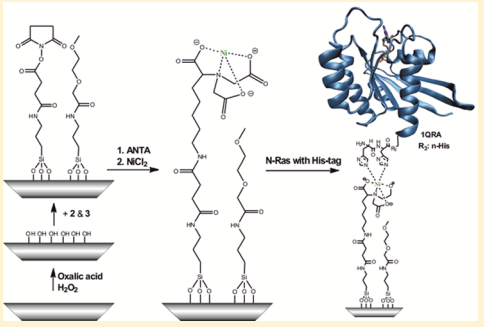

INTRODUCTION

Analyzing the molecular reaction mechanisms of proteins or their interaction with small molecules or other proteins at atomic detail is an emerging field. Techniques based on immobilized proteins achieve success since they allow investigation of the interaction of proteins with different molecules, drugs, or proteins in varying conditions and concentrations.[1−4] Fluorescence-based methods have an excellent signal-to-noise ratio and can deal with low sample concentrations.[5−7] On the other hand, surface plasmon resonance is a widely used label-free technique that detects mass changes at the sensor surface.[8] Label-free methods are becoming increasingly popular as the attached label can interfere with the reaction and the labeling is an extra step that is often difficult to handle. Attenuated total reflection Fourier transform infrared (ATR-FTIR) spectroscopy is a label-free method that can be used in a similar manner as surface plasmon resonance but provides the structural detail of vibrational spectroscopy, which reveals additional detailed information (e.g., on the structure, reaction mechanism, protonation states, hydrogen bonding, or orientation).[9−12] To achieve a sensitivity that allows the observation of individual functional groups in a reaction by ATR-FTIR spectroscopy, effective immobilization strategies must be applied. We recently reported an immobilization technique based on noncovalently attached single lipid bilayers.[13] Although the lipid bilayer might mimic a more native environment for lipid-anchored proteins, the noncovalent nature of the surface attachment prevents the immobilization of transmembrane proteins. The lipid bilayer is not stable in the presence of detergents. This can be overcome using covalent binding; thus, chemical modification of the ATR surface is necessary.

Although such modifications of silicon surfaces are relatively well established, only few attempts have been made for the most suitable IR waveguide material, germanium. Germanium can be directly functionalized by chlorine or hydrogen termination or by silanization.[14] Germanium is superior to silicon for FTIR applications for two reasons. First, the refractive index is larger, which leads to a better signal-to-noise ratio in thin film experiments.[15] Second, and most important, the spectroscopic window in the mid-IR fingerprint

Received: January 9, 2013
Published: February 15, 2013

region is much larger, ranging down to 830 cm^{-1} compared to 1470 cm^{-1} for silicon.[10] Thus, absorption bands from important functional groups like phosphates are not detectable using silicon. Here we present an improved methodology for the chemical modification of germanium by silanization. All surface modification steps can be performed within a flow-through system inside the spectrometer at room temperature. This allows for direct monitoring of the generation of the self-assembled monolayer (SAM). The resulting SAM is stable under aqueous conditions for many days. Here we use nitrilotriacetic acid (NTA)-terminated linker molecules, allowing repetitive immobilization and removal of His-tag proteins, which are usually easy to obtain. We demonstrate the capability of our system by showing results from a soluble protein (Ras)[16] and a transmembrane protein (photosystem I, PS I).[17,18] The signal-to-noise ratios of the obtained difference spectra from monolayers are outstanding and allow probing protein reaction mechanisms at the atomic level.

EXPERIMENTAL SECTION

Materials. All chemicals were purchased from Sigma-Aldrich (Taufkirchen, Germany). Solvents were used in HPLC-grade (Sigma-Aldrich). N-Ras1−180 with a C-terminal decahistidine-tag was expressed as described for N-Ras without the His-Tag,[19] and purified using immobilized metal ion affinity chromatography (IMAC) and size exclusion chromatography. H-Ras1−166 without the His-tag was used in control experiments and was prepared as described elsewhere.[19] PS I was expressed and prepared as described previously.[20] In contrast to the preparation of wild-type PS I, an IMAC was performed followed by hydrophobic interaction chromatography.

*Synthesis of N-(4,4,4-Triethoxysilanebutyl)succinamic Acid (**1**).* In a 250-mL three-necked-flask, 1 g (9.9 mmol) of succinic anhydride was dissolved in dry 1,4-dioxane at 60 °C under an argon atmosphere. At room temperature, 2.1 mL (9.0 mmol) of (3-aminopropyl)-triethoxysilane in 10 mL of 1,4-dioxane were added dropwise. The solution was stirred for 1 h and then filtered. After the evaporation of the solvent, a colorless oil was obtained and characterized. FTIR (cm^{-1}): 3294 (NH), 2975 (CH_3), 2929 (CH_2), 2880 (CH_2), 1717 (CO, acid), 1640 (CO, amide I), 1545 (NH, amide II), 1069 (Si−O−Et). ^{1}H NMR (ppm) (200 MHz, $CDCl_3$): δ 0.56−0.64 (t, 2H), 1.15−1.22 (t, 9H), 1.50−1.66 (m, 2 H), 2.44−2.50 (t, 2H), 2.60−2.71 (t, 2H), 3.15−3.25 (m, 2H), 3.77−3.89 (q, 6H), 6.58−6.64 (s, 1H), 10.39−10.88 (s, 1H). ^{13}C NMR (ppm) (200 MHz, $CDCl_3$): δ 7.7 (s), 18.2 (s), 22.6 (s), 30.1 (s), 30.7 (s), 42.3 (s), 58.6 (s), 172.5 (s), 175.6 (s). FAB-MS: 322.2 [M + H^+], 344.1 [M + Na^+] [M ($C_{13}H_{27}NO_6Si$) = 321.2 g/mol].

*Synthesis of N-(4,4,4-Triethoxysilanebutyl)succinamic Acid 2,5-Dioxopyrrolidin-1-yl Ester (**2**).* In a 250-mL three-necked-flask, 1 g of **1** (3.11 mmol) was dissolved in dry 1,4-dioxane under an argon atmosphere. The mixture was stirred and 536.3 mg (4.66 mmol) of *N*-hydroxysuccinimide (NHS) and 769.6 mg (3.73 mmol) of dicyclocarbodiimide (DCC) were added. After 3.5 h, the insoluble urea derivative was removed by filtration and the residue was evaporated. The filtration was repeated if traces of the reactants could be detected by FTIR. The white product was dried in vacuum and characterized. FTIR (cm^{-1}): 3305 (NH), 2974 (CH_3), 2927 (CH_2), 2886 (CH_2), 1813 (CO, imide), 1779 (CO, imide), 1733 (CO ester), 1642 (CO, amide I), 1556 (NH, amide II), 1066 (Si−O−Et). ^{1}H NMR (ppm) (200 MHz, $CDCl_3$): δ 0.59−0.66 (t, 2H), 1.19−1.26 (t, 9H), 1.50−1.66 (m, 2H), 2.54−2.60 (t, 2H), 2.83−2.86 (s, 4H), 2.95−2.99 (t, 2H), 3.20−3.30 (m, 2H), 3.77−3.88 (q, 6H), 6.05−6.10 (s, 1H). ^{13}C NMR (ppm) (200 MHz, $CDCl_3$): δ 7.7 (s), 18.2 (s), 22.9 (s), 24.6 (s), 27.0 (s), 33.7 (s), 49.9 (s), 58.6 (s), 168.1 (s), 168.8 (s), 176.8 (s). FAB-MS: 419.2 [M + H^+], 441.2 [M + Na^+] [M ($C_{17}H_{30}N_2O_8Si$) = 418.2 g/mol].

*Synthesis of 2-(2-Methoxyethoxy)-N-(4,4,4-triethoxysilanebutyl)-acetamide (**3**).* In a 100-mL three-necked-flask, 1 g (7.46 mmol) of 2-(2-methoxyethoxy)acetic acid was dissolved in dry tetrahydrofuran (THF) under argon atmosphere. A solution of 1.27 g (11.1 mmol) of NHS and 1.84 g (8.94 mmol) of DCC in THF was added quickly. After 4.5 h, the insoluble urea derivative was separated and the residue was evaporated. In 100 mL of dry THF, 2.1 mL (9.0 mmol) of 3-aminopropyltriethoxysilane and 1.23 mL (9.0 mmol) of triethylamine were added to the activated compound. The mixture was stirred under argon for 5 h. The filtration was repeated if traces of the reactants could be detected by FTIR. The slightly yellow oil product was dried in vacuum and characterized. FTIR (cm^{-1}): 3325 (NH), 2979 (CH_3), 2929 (CH_2), 2849 (CH_2), 1671 (CO, amide I), 1554 (NH, amide II), 1051 (Si−O−Et). ^{1}H NMR (ppm) (200 MHz, DMSO-d_6): δ 0.49−0.57 (t, 2H), 1.12−1.19 (t, 9H), 1.40−1.56 (m, 2 H), 3.0−3.14 (m, 2H), 3.25−3.31 (s, 3H), 3.46−3.51 (t, 2H), 3.56−3.61 (t, 2H), 3.70−3.80 (q, 6H), 3,86 (s, 2H), 7.61−7.64 (s, 1H). ^{13}C NMR (ppm) (200 MHz, $CDCl_3$): δ 7.3 (s), 18.1 (s), 22.7 (s), 25.1 (s), 57.7 (s), 58.1 (s), 69.9 (s), 70.1 (s), 71 (s), 168.9 (s). FAB-MS: 338.2 [M + H^+], 360.1 [M + Na^+] [M ($C_{14}H_{31}NO_6Si$) = 337.2 g/mol].

Preparation of Germanium. ATR-FTIR measurements were performed as described previously.[21] The internal reflection elements (IREs) were 52 × 20 × 2 mm^3 trapezoidal germanium ATR plates with an aperture angle of 45°. We used one side of the IRE for surface functionalization, resulting in 13 active reflections. First, the IRE was cleaned with water and polished.[21] Activation was achieved by immersing the IRE in H_2O_2 (30%) and saturated oxalic acid (9:1) for 5 min. Subsequently, the IRE was dried with nitrogen and washed with water. This procedure was repeated three times (modified after Devouge et al.).[22] The hydroxylated IRE was placed in a cuvette and immediately placed in the FTIR spectrometer (Bruker Vertex 80 V). The surface was flushed with 2-propanol until the system was equilibrated as indicated by a stable spectrum.

Surface Functionalization. The synthesized compounds **2** and **3** were dissolved in 2-propanol. To ensure complete solubilization, the solution was sonicated. The final concentrations of silanes **2** and **3** were 300 μM for all ratios. The coverage density could be controlled by the use of different ratios. After the completion of the reaction (monitored by ATR-FTIR) the IRE was washed with 2-propanol to remove unbound compounds.

Coupling with ANTA. The reaction with aminonitrilotriacetic acid (ANTA) has to be carried out under aqueous conditions. Therefore, the 2-propanol was removed by immersing the surface with water and finally with potassium carbonate buffer (500 mM, pH 9.8).[23] The 2 mM ANTA solution was applied immediately after the buffer exchange to avoid hydrolysis of the succinimidyl ester. The reaction with ANTA was done overnight, and a surface with high specificity toward a His-tag was obtained.

Immobilization of His-Tag Ras and PS I. Before changing the ANTA coupling buffer to the desired protein-binding buffer, the surface was washed for 30 min with Millipore water. For Ras immobilization, protein-binding buffer 1 [50 mM Tris (pH 7.4), 100 mM NaCl, 1 mM $NiCl_2$, 1 mM $MgCl_2$, and 0.1 mM GDP] was used. For immobilization of photosystem I, protein-binding buffer 2 [50 mM Tris (pH 8.0), 0.1% β-dodecylmaltoside, and 1 mM $NiCl_2$] was used. A background spectrum was recorded before the addition of the protein. His-tagged proteins were added to a final concentration of 1.8 μM in the case of Ras [1.0 μM in half-maximal effective concentration (EC_{50}) experiments] and 43 nM in the case of PS I. If not stated otherwise, in the case of Ras a surface with 100% linker−silane and for PS I a surface with 50% linker−silane and 50% matrix silane was used. After recording the binding process for approximately 1 h, the surface was flushed with buffer until no dissociation of the protein was observed. The immobilized proteins were then analyzed by difference spectroscopy, where a perturbation was either light-induced or caused by small molecule interactions. Light-induced difference spectroscopy of PS I was performed by collecting 1000 scans in the dark for the reference spectrum, followed by illumination of the surface by a cold light source (Fiberoptic Heim LG 2600) and subsequently collecting 1000 scans for the sample spectrum after 10 s of light adaption.

ATR-FTIR. ATR-FTIR measurements were performed as described previously.[21] Briefly, we used a Vertex 80 V spectrometer (Bruker

Optik, Ettlingen, Germany) at 293 K, with a spectral resolution of 2 cm^{-1} and a scanner velocity of 80 kHz (0.025 m s^{-1}); scans were performed in the double-sided forward–backward mode. The resulting interferograms were apodized with the Blackman–Harris three-term function and with a zero-filling factor of 4. For the polarized measurements of the silane binding reaction and the bound PS I a gold-grid polarizer (Specac, Orpington, UK) was used. For the silane binding spectra and kinetics the parallel polarized data are shown here.

X-ray Photoelectron Spectroscopy (XPS). The IREs were cut into three pieces to adapt them for the sample holder. XPS was performed in an ultrahigh vacuum (UHV) setup equipped with a Gammadata-Scienta SES 2002 analyzer. The base pressure in the measurement chamber was 5×10^{-10} mbar. Monochromatic Al Kα (1486.6 eV, 14.5 kV, 30 mA) was used as incident radiation, and a pass energy of 200 eV was chosen, resulting in an effective instrument resolution higher than 0.6 eV. Charging effects were compensated using a flood gun, and binding energies were calibrated on the basis of positioning the Ge $3d_{5/2}$ signal at 30.1 eV. Measured data were fitted using Shirley-type backgrounds and a combination of Gaussian–Lorentzian functions with the Casa XPS software.

RESULTS AND DISCUSSION

We report on the chemical modifications of germanium surfaces that allow for the specific attachment of proteins via a His-tag. The application of this technique to ATR crystals enables the immobilization of proteins on the IR waveguide and thereby allows infrared studies of proteins and their respective reaction mechanisms, even in the case of ligand-induced reactions. We first describe the syntheses of the precursor molecules. Then, we report on the chemical modification of germanium by subsequent synthesis steps, which were monitored stepwise within the spectrometer using a flow-through setup. Finally, we applied our Ni–NTA-based immobilization technique to N-Ras and PS I and obtained high-quality difference spectra.

Synthesis of Linker– and Matrix–Silanes. The first step was the organic synthesis of the linker–silane **2** and a matrix–silane **3** (Scheme 1). The linker molecule was synthesized by the coupling of (3-aminopropyl)triexthoxysilane with succinic anhydride, which leads to a terminal carboxylic acid. The product (compound **1**) was then incubated with NHS and DCC to form the activated succinimidyl ester. The synthesis of **3** was achieved by the reaction of (3-aminopropyl)-triexthoxysilane and (2-methoxyethoxy)acetic acid in the presence of NHS and DCC. For all synthesis steps, the exclusion of water was essential, because water would convert the triethoxysilane into trihydroxysilane, which cannot bind to the germanium surface. All products were characterized using ^{1}H NMR, ^{13}C NMR, FAB-MS, and FTIR (NMR spectra are shown in the Supporting Information).

Scheme 1. Reaction Scheme for the Synthesis of Compounds 1–3

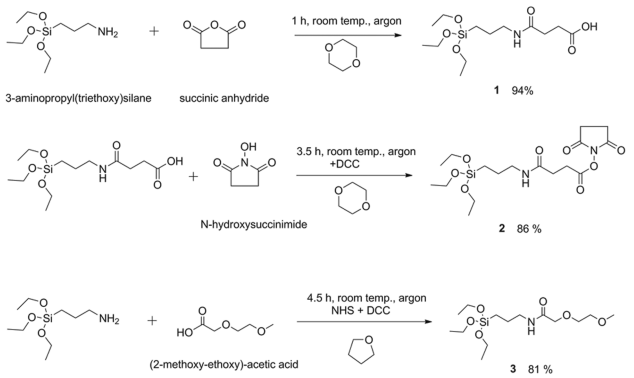

Surface Functionalization. For our ATR-FTIR setup, we used germanium crystals as the IRE. We modified the procedure reported by Devouge et al.[22] and activated the germanium crystals using hydrogen peroxide (30% p.a.) and oxalic acid (saturated solution) to form a hydroxyl-terminated layer. The germanium crystal was then fixed in a flow-through cuvette within an FTIR spectrometer, and the cuvette was flushed with 2-propanol. 2-Propanol was chosen as the solvent because it has good solubility with regard to the silanes and high miscibility with water, which is important for the later steps. A background spectrum was recorded after 45 min of rinsing the surface with 2-propanol, and subsequently, a solution of the respective silane mixture dissolved in 2-propanol was pumped through the cuvette and a time course of sample spectra was recorded. The incubation resulted in the covalent binding of **2** and **3** to the surface, as monitored by infrared absorption (Figure 1). After the addition of compound **2**, characteristic bands could be detected at 1550, 1658, 1698, 1738, and 1780 cm^{-1}.

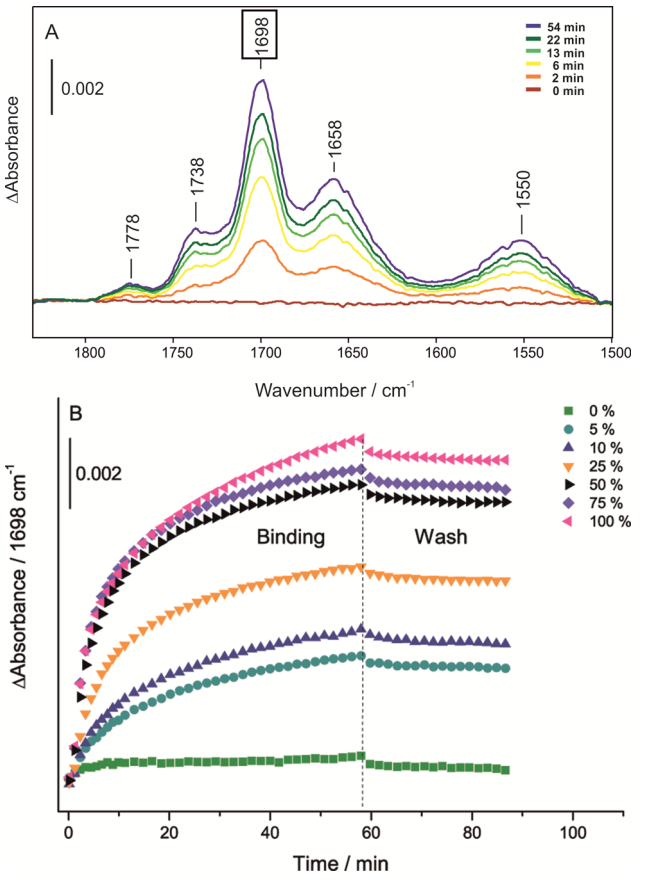

Figure 1. (A) FTIR spectra of the surface functionalization (50% linker–silane) reaction of the germanium IRE by silanes at several times. (B) Silane-binding kinetics at different ratios of succinimidyl ester triethoxysilane (linker) and ethylenglycol triethoxysilane (spacer). The data is color coded with respect to the percentage of the linker concentration. The absorption at 1698 cm^{-1} increases with increasing concentration of the succinimidyl ester triethoxysilane. All concentrations of linker and spacer showed similar binding kinetics and stable attachment.

dx.doi.org/10.1021/ja400253p | J. Am. Chem. Soc. 2013, 135, 4079–4087

We assigned the band at 1698 and 1780 cm^{-1} to the succinimidyl ring, and the band at 1738 cm^{-1} to the ester bond (Figure 1A).[24] The bands at 1658 and 1550 cm^{-1} are well-known as amide I (CO stretching) and amide II (NH bending, CN stretching). Unfortunately, the absorptions of the Si−O stretching vibration are masked by absorptions of the solvent 2-propanol. During the reaction 2-propanol is displaced, as indicated by two negative peaks at 2971 cm^{-1} and 3315 cm^{-1} (Figure S1, Supporting Information). Kinetic analysis of the reaction was carried out by plotting the absorbance of the band at 1698 cm^{-1} against time (Figure 1B). After about 50 min, the reaction was almost complete, and unreacted compounds were removed by washing with 2-propanol. For the adjustment of the surface density of the linker, different ratios of linker−silane and matrix−silane were used. The intensity of the NHS-characteristic band at 1698 cm^{-1} increases with linker concentration (Figures 1B and S2, Supporting Information). On the other hand, the amide I absorbance is nearly independent of the mixing ratio, since both silanes contain a peptide group. Each of the three silicon-coupled ethoxy groups can react with one hydroxyl group on the germanium surface. Hydrogen bridges are expected between the amide groups of attached molecules, forming a hydrophobic barrier that prevents hydrolysis.[22] This is supported by the observation that the surface is stable over many days. Therefore, our functionalization of germanium leads to a stable modified surface, even under aqueous conditions.

Characterization by XPS. Furthermore, the linker- and matrix−silane-modified germanium crystals were characterized by X-ray photoelectron spectroscopy. Comparability between the different samples was achieved by normalization to the integral peak area of the intense Ge 3d signal. Additionally, the binding energy was calibrated to the Ge $3d_{5/2}$ signal at 30.1 eV.[25] The C 1s signal of the matrix−silane-modified sample exhibits four different signals at 285.4, 286.1, 287.3, and 288.9 eV, which were fitted by Gaussian−Lorentzian functions using a Shirley-type background (Figure S3A, Supporting Information). The peaks were attributed to carbon atoms in *C*−H (285.4 eV), *C*−N and *C*−C(O)−N (286.1 eV), *C*−O (287.3 eV), and *C*(O)−N (288.9 eV) configurations. The peak positions are in good agreement with previously reported binding energies of similar compounds.[26] The carbon of the alkyl chain is slightly shifted toward higher binding energies. The atomic concentrations of the different carbon compounds derived from XPS analysis are in good agreement with the theoretical values of the matrix−silane molecule (Table 1). In case of the linker−silane, adequate peak fitting could be achieved using a model consisting of four different carbon compounds belonging to the linker−silane and an additional peak representing carbon contamination at the germanium crystal (Figure S3B, Supporting Information). As expected, a similar contamination was also observed for the activated, hydroxyl-terminated germanium surface after hydrogen peroxide and oxalic acid treatment. However, the peak positions of *C*−H (285.2 eV), *C*−N and *C*−C(O)−N (286.1 eV), *C*−C(O)−O (286.9 eV), *C*(O)−N (288.5 eV), and *C*(O)−O-like (289.5 eV) carbons were in good agreement with previous reports.[26] Furthermore, the experimental atomic concentrations match the theoretical atomic concentrations of the different carbon compounds (Table 1).

Table 1. Atomic Concentrations of the Different Carbon Compounds of the Matrix− and Linker−Silane-Modified Germanium Crystal Surface, Determined by XPS Analysis

	100% matrix−silane		100% linker−silane	
	exptl (atom %)	theor (atom %)	exptl (atom %)	theor (atom %)
C 1s CC	23.5	25.0	23.5	18.2
C 1s CN + α-carbon CNOH	26.6	25.0	20.1	18.2
C 1s C−O	39.0	37.5	–	–
C 1s CNOH	11.0	12.5	9.0	9.1
C 1s α-carbon COOR	–	–	28.5	27.3
C 1s COOR	–	–	18.7	27.3

Formation of Ni−NTA. The attached succinimidyl esters were used for the reaction with the primary amine amino-nitrilotriacetic acid (ANTA).

For the coupling, 2-propanol was removed by rinsing for 5 min with water and K_2CO_3 buffer (500 mM, pH 9.8).[23] Subsequently, a solution of 2 mM ANTA in K_2CO_3 buffer was used and after 5 min a new background was recorded. Bound ANTA was characterized by four bands, increasing in intensity over time: the bands caused by the symmetric stretching of the seven additional CH_2 groups at 2852 cm^{-1}, amide I (C═O stretching vibration, 1645 cm^{-1}), amide II (NH bending vibration, 1553 cm^{-1}), and the symmetric stretching of the three deprotonated carboxylic acids coupled with the C−N stretching and the C−H bending vibration from 1441 to 1400 cm^{-1} (Figure 2A).[23] During the reaction displaced water molecules were detected by the negative signal at 3375 cm^{-1}. The band at 2852 cm^{-1} was plotted against time, because no interference with the water-bending vibration occurs in this region. Completion of the reaction took approximately 13 h. The complete reaction of all succinimidyl esters is important to ensure a high surface concentration of NTA groups. Further, the lysine side chains of the protein might react in subsequent steps, which could damage the protein. Before the addition of His-tagged protein, the surface was immersed with 1 mM $NiCl_2$ in the desired buffer. The nickel cation was coordinated by the three carboxylic acids and the nitrogen atom and thereby prepared the surface for the attachment of any His-tagged protein.

To further confirm the successful transformation of the succinimidyl esters, the transformed and Ni-loaded sample was characterized by XPS. The peak shape of the C 1s signal is altered upon ANTA modification, indicating a successful reaction (Figure 3). It is striking that the C 1s signal of the carboxylic carbon (COOR), observed at 289.5 eV for the unmodified linker−silane germanium crystal (C4* in Figure S3B, Supporting Information), shifted toward lower binding energy and could be observed at 289.0 eV instead (C4 in Figure 3). Additionally, at lower binding energy (C3, 287.2 eV), a shoulder was observed, which can be attributed to an α-carbon adjacent to the carbonylic carbon in C−C(O)-O and the carbonylic carbon in the C−C(O)-N configuration. Comparison to the unmodified linker−silane sample revealed that the carbonylic C−C(O)-O carbon is shifted to a higher binding energy, whereas the carbonylic carbon in the C(O)−N configuration is shifted to lower binding energy, resulting in an overlap of the two signals. Finally, an increase in the carbon signal belonging to carbon in an aliphatic hydrocarbon chain was observed (C1 carbon signal in Figure 3 compared with C1* in Figure S3B, Supporting Information). The shift in binding energy of the carboxylic carbon upon Ni modification can be explained by an ionic interaction. The shift toward higher

dx.doi.org/10.1021/ja400253p | J. Am. Chem. Soc. 2013, 135, 4079−4087

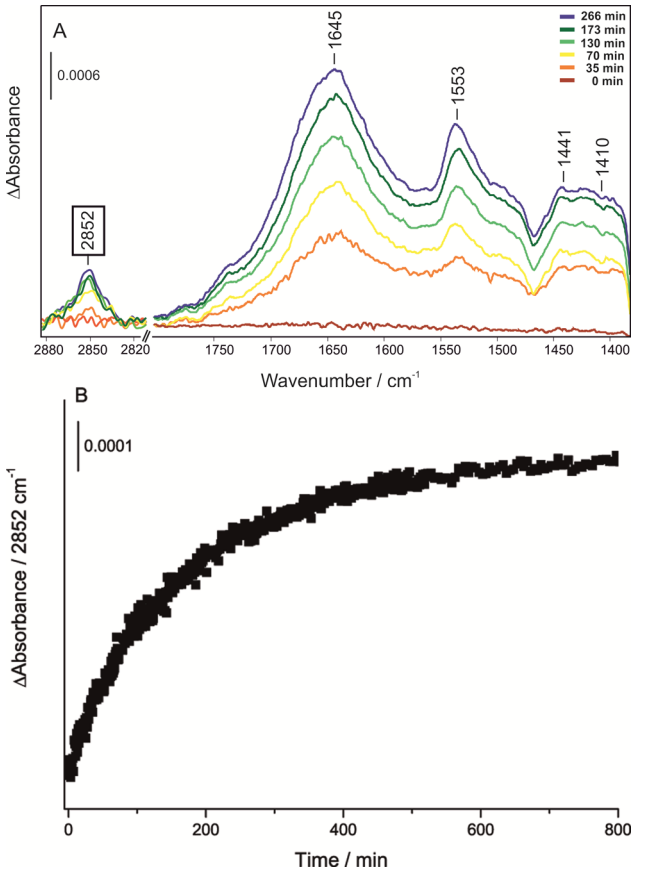

Figure 2. (A) Formation of the histidine-affinity surface by the reaction of aminonitrilotriacetic acid with the succinimidyl ester (compound **2**). Characteristic bands are labeled in the FTIR spectra. (B) Kinetic analysis of the reaction was carried out using the absorption band of the CH_2-stretching mode at 2852 cm^{-1}, because no interference with the water-bending vibration occurs in this region.

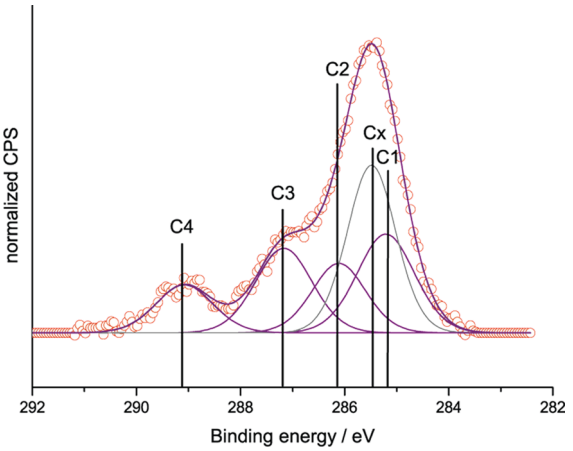

Figure 3. C 1s signal of a germanium crystal with a histidine-affinity surface. The carbon signal was fitted using Gauss–Lorentzian functions; proper fitting was achieved using a model based approach. The different carbon species were assigned to the following species: C1 corresponds to carbon in an alkyl chain (C–H), C2 is due to *C*–N– and *C*–C(O)–N-like species, C3 was assigned to *C*–C(O)–O and the carbonylic carbon in the *C*(O)–N-like carbon species, and C4 represents the carboxylic carbon *C*(O)–OR. Cx is due to carbon contamination on the germanium surface.

binding energies of the carbonylic *C*–C(O)–O carbon can be explained by the neighboring nitrogen atom. Therefore, the shifts and the increase in the aliphatic hydrocarbon signal (C1 in Figure 3) are in good agreement and indicate the successful reaction of the succinimidyl esters with ANTA. The fit shown in Figure 3 is consistent with 100% coupling efficiency. However, due to the carbon contamination (Cx) we cannot rule out up to 30% of hydrolysis side reaction. No characteristic Ni signal could be detected in the survey spectra, which can be explained by the low Ni concentration and high background in this region due to strong Ge signals. In comparison to the Ni-unmodified samples, the background of the survey spectra is more intense in the higher energy region. This, however, is evidence of an additional compound in the sample. It should be mentioned that a proper fitting of the C 1s signal was only possible using an additional carbon compound assigned to contaminating carbon, which is commonly observed due to contamination by pump oil. The atomic concentration of the contamination is similar to the atomic concentration detected for the linker–silane (~35 atom %).

Immobilization of His-Tagged Proteins. After the preparation of the germanium surface, a background spectrum of protein-binding buffer 1 was measured. N-Ras with a C-terminal decahistidine-tag was introduced in the flow system to a concentration of 1.8 μM. The attachment could be followed over time as an increase in intensity of the amide I and amide II bands (Figure 4A). The shape of the amide I band indicates a native protein, as shown in Figure S4 (Supporting Information);[13] Ras consists of larger α-helical regions and smaller β-sheet regions.[27]

Surface Characteristics. The surface density of the protein can be controlled by varying the linker concentration. With 10% linker, most proteins will bind to only one NTA group, which leads to less stable binding. When more Ni–NTA groups (e.g., 100%) are available, the amount of immobilized N-Ras can be increased, because most proteins are now multibinders (Figure S5, Supporting Information). The kinetics of the attachment was analyzed by plotting the absorption of the amide II band against time in Figure 4B. Selected data points in the spectra (A) and the kinetic profile (B) are labeled in orange (12 min) and red (53 min). After about 50 min, the coverage of the surface was sufficient. To remove the loosely bound nonmultibinder proteins, the surface is washed until the protein layer is stable at about 20 mOD. To control the specificity of the immobilization, H-Ras1–166 without the His-tag was flushed over the surface (Figure 4B, dark green). The adsorption kinetic of the protein shows that a small amount (<20%) of the bound protein was irreversibly bound. A similar amount of this nonspecific binding was found in the control experiments using matrix–silanes carrying no NTA groups (Figure 4B, red). However, once the nonspecific binding sites are blocked, further nonspecific binding is negligible, as can be seen from the repetitive incubation with Ras (Figure 4B, light green) after regenerating the surface with 200 mM imidazole and 0.1% sodium dodecyl sulfate (SDS). Nonspecific binding is irrelevant for activity assays revealed by difference spectroscopy, because only the action of the native protein is seen in the spectra.

On the basis of the absorption of the amide II region, we estimated the surface concentration of Ras in our experiments to be 22 pmol/cm^2 and of PS I to be 1.14 pmol/cm^2 (Supporting Information). These values are within the expected error margin compared to the calculated theoretical surface

dx.doi.org/10.1021/ja400253p | J. Am. Chem. Soc. 2013, 135, 4079–4087

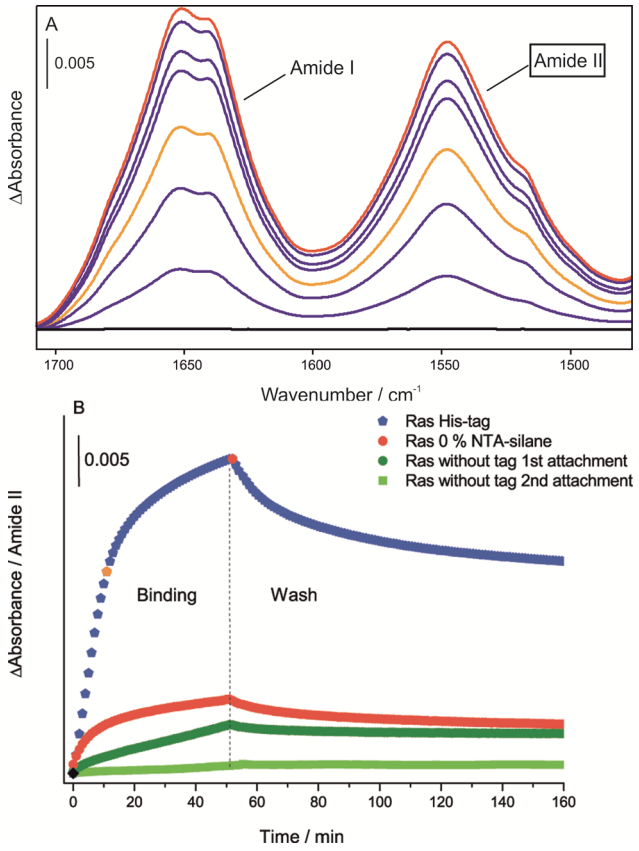

Figure 4. (A) Binding of His-tagged N-Ras to a Ni–NTA surface (100% linker–silane). (B) In the FTIR spectra and kinetic analysis, selected time points are labeled in orange (12 min) and red (53 min). Without Ni–NTA groups (red) or without the His-tag (dark green), only a small amount of nonspecific binding is detected. In a repeated incubation, the amount of nonspecific bound protein was significantly decreased (light green).

concentrations of a monolayer of 19.4 pmol/cm^2 for Ras and 1.4 pmol/cm^2 for PS I, respectively.

Specificity of Immobilization, Stability, and Reusability of the Surface. To check the long-term stability of the NTA surface we performed repeated association and dissociation of Ras with 200 mM imidazole, which is shown in Figure 5. Over 80% of the attached protein could be removed in the first cycle by imidazole treatment, indicating that more or less all of the specifically bound protein is removed. In repeated attachments, over 90% of the surface-attached Ras molecules could be removed by imidazole. This is most likely due to the blocking of nonspecific binding sites described above. The repeated association and dissociation of Ras showed almost identical binding kinetics (Figure 5), emphasizing the robustness of the generated surface. To further characterize the affinity, the EC_{50} value for imidazole was measured according to the literature.[28] We obtained a value of 6 mM imidazole. The resulting protein attachment is sufficiently stable for difference spectroscopic analysis (Figures S6 and S7, Supporting Information). Multibinding is important for increasing the affinity, as shown for freely diffusible NTA groups bound to lipids[13] and can be enhanced by using multiple NTA groups.[28] The chemically modified surface can be used for a week with no difference in the attachment and activity of the protein. For complete regeneration, the surface is flushed with 200 mM imidazole and 0.1% SDS overnight. This

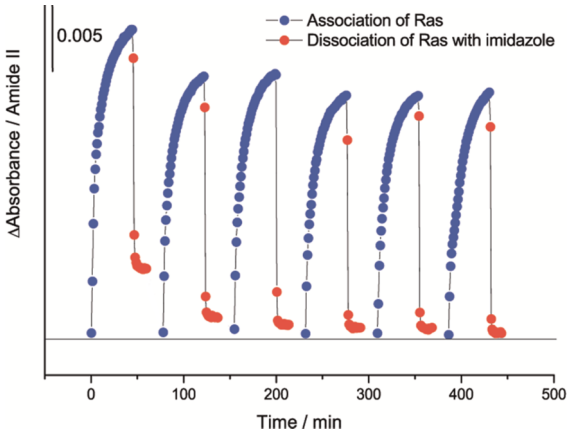

Figure 5. Reversible Immobilization of N-Ras on the generated Ni–NTA surface. N-Ras was repetitively incubated and washed off the surface with 200 mM imidazole.

makes the measurement more convenient, because repeated preparation of the chemically functionalized surface is not necessary.

Difference Spectroscopy of Soluble Proteins. In cells, Ras acts as a molecular switch between the "on" state with bound GTP and the "off" state with bound GDP. The immobilized Ras is first in the off state with GDP in the nucleotide binding pocket. To study its activity, a beryllium trifluoride anion titration assay was performed. Beryllium trifluoride anion functions as a γ-phosphate analogue and promotes the transition from the off to the on state by binding to GDP-Ras. The on state is characterized by the marker band of threonine-35 (1689 cm^{-1}, Thr35).[29] Further information is revealed by the β-phosphate band. The positive band at 1157 cm^{-1} indicates the Ras–GDP–BeF_3^- state and the negative band at 1136 cm^{-1} the Ras–GDP state. Hence, by switching between different concentrations of BeF_3^- (0–4 mM), the function of Ras as molecular switch could be demonstrated (3D difference spectra, Figure 6). The corresponding infrared difference spectrum is almost identical to the one obtained for lipidated N-Ras bound to a POPC model membrane (Figure S8, Supporting Information).[12] The ability of our technique to immobilize proteins in a native and fully active way and to monitor their conformational changes upon ligand interaction is hereby demonstrated.

Difference Spectroscopy of Transmembrane Proteins. After establishing the technique for the soluble protein Ras, we applied it to a member of the more challenging protein class of transmembrane proteins. Therefore, we studied the immobilization of PS I. The PS I construct used has a decahistidine-tag at the PsaF subunit for attachment.[20] The great advantage of the chemically modified surface in contrast to immobilization techniques based on solid-supported lipid bilayers is the possibility of working with proteins in detergent micelles and to be nearly unlimited in the use of chemicals in the buffer solution. The surface was prepared in the same way as for Ras immobilization, but the protein binding buffer 2 was supplemented with 0.1% β-dodecylmaltoside. Before the addition of PS I, a new background was recorded. Immediately after the addition of PS I to a concentration of 43 nM, two major amide bands appeared, which increased in intensity over time. The binding process was almost complete after 20 min, and loosely bound protein was washed away by flushing the surface with buffer for 60 min (Figure 7B). The amide II band

dx.doi.org/10.1021/ja400253p | J. Am. Chem. Soc. 2013, 135, 4079–4087

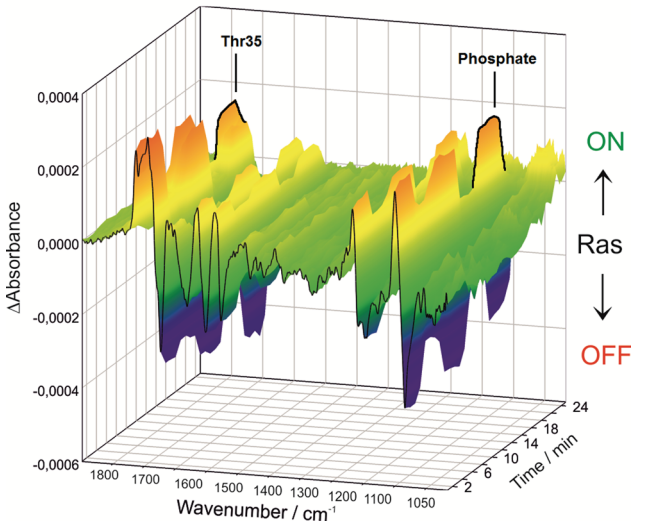

Figure 6. 3D-difference spectra of the interaction of Ras–GDP with the small molecule beryllium fluoride (BeF_3^-). This compound mimics the γ-phosphate and induces the conformational change from the off state to the on state, which is indicated by the marker band of Thr35. By switching between buffers with different concentrations of BeF_3^- (0–4 mM), the on and off states can be obtained.

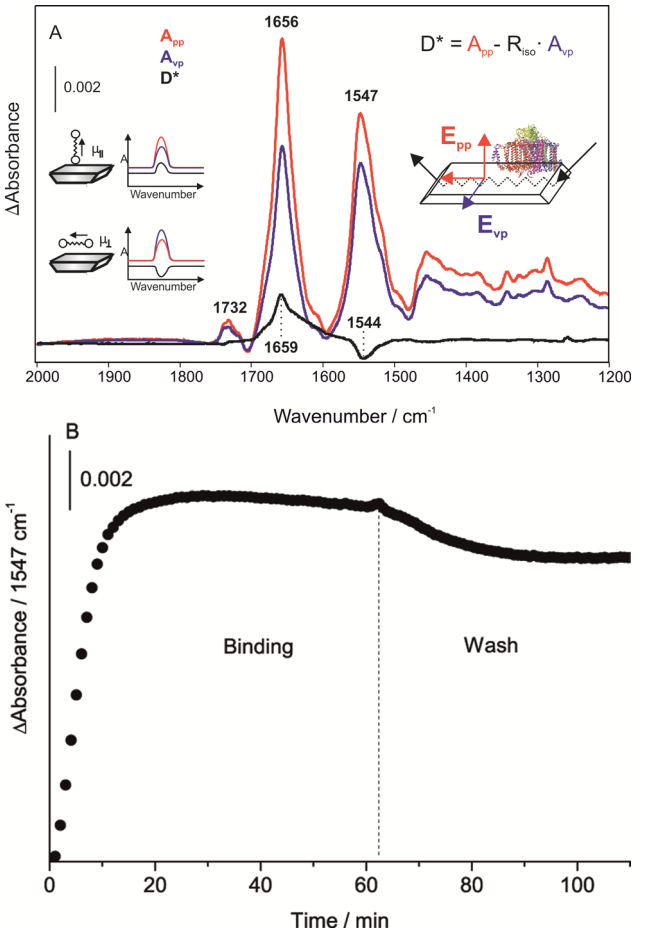

Figure 7. (A) Information on the orientation of immobilized proteins can be gained by using polarized infrared light (E_{pp} and E_{vp}). Transition dipole moments parallel to the perpendicular of the ATR crystal (μ II) interact more strongly with E_{pp}, resulting in a greater absorption (A_{pp}) compared to A_{vp}, leading to a positive peak in the dichroic difference spectrum (D*). On the other hand, absorptions resulting from transition dipole moments parallel to the surface (μ I) interact more strongly with E_{vp}, resulting in a negative peak in D*. In D* of PS I, a positive peak at 1659 cm^{-1} indicates that the majority of the transition dipole moments of the helical parts of the protein are perpendicular to the surface. (B) Binding kinetic of PS I adsorbing at the Ni–NTA surface (50% linker–silane).

decayed in 30 min to 85% of the maximum load and remained stable over 24 h. The amide I band showed the characteristic position for α-helical structures at 1656 cm^{-1}, the amide II band appeared at 1547 cm^{-1}, and a third band was detected at 1732 cm^{-1}, which is typical for the C=O bond in esters, as in the lipid membrane (Figure 7A). The differences in the shape of the amide I band of the proteins N-Ras and PS I are characteristic for the different secondary structure compositions of both proteins (Figure S9, Supporting Information). Whereas Ras consists of α-helices and β-sheets, PS I is nearly completely α-helical. Thus, Ras showed a broader absorption with a maximum at 1650 cm^{-1}, but PS I showed an absorption maximum at 1656 cm^{-1}, the typical wavenumber for α-helices (Figure S9, Supporting Information). Our universal technique shows direct hints concerning the structure of the protein. Denatured or unfolded proteins can be discriminated from native proteins, because of their different amide bands. Imidazole alone was not sufficient to elute PS I from the surface, presumably because a closed detergent–protein layer shields the NTA groups. The disruption of this layer by 0.02% SDS enables imidazole to displace PS I from the surface.

Here, we performed dichroic ATR measurements by recording spectra with parallel (A_{pp}) and vertical (A_{vp}) polarized beams with respect to the perpendicular of the surface. The scaled difference of both spectra, the so-called dichroic difference spectrum (D*), was calculated using a constant R_{iso} of 1.72, as described elsewhere[21], and can be used to interpret the molecular orientation of the absorbing transition dipole moments. In the case of α-helices, a positive band in the amide I region and a negative band in the amide II region is caused by α-helices vertically oriented to the IRE.[21] This spectral pattern of D* was observed also for immobilized PS I, indicating that the protein, which consists predominantly of α-helices, is oriented with its helices vertical to the IRE surface, as shown in Figure 7A.

Immobilized PS I was illuminated by a cold light source, and a light-induced difference spectrum was obtained (Figure 8). The difference spectrum is fully in accordance with the literature.[30] As discussed by Iwaki et al., the difference bands can be interpreted as the activity of the special pair (chlorophyll dimer) P_{700}. The largest difference band, at 1718/1700 cm^{-1}, is caused by positive charge-induced changes in the non-hydrogen-bonded keto and ester C=O groups of one chlorophyll from the special pair. In summary, we have shown for the first time dichroic binding spectra of the native immobilization of a detergent-solubilized membrane protein and the subsequent infrared difference spectroscopic characterization of the activity of the protein.

Comparison with Other Immobilization Techniques. As discussed in the Introduction, only a few attempts have been made for the covalent attachment of linker molecules on germanium, which is the best material for ATR-FTIR spectroscopy. Attempts have been made for NTA immobilization of peptides by depositing a thin layer of gold–palladium alloy or SiO_2 on germanium IREs and subsequently functionalizing those surfaces using thiols or silanes.[31] Some

dx.doi.org/10.1021/ja400253p | J. Am. Chem. Soc. 2013, 135, 4079–4087

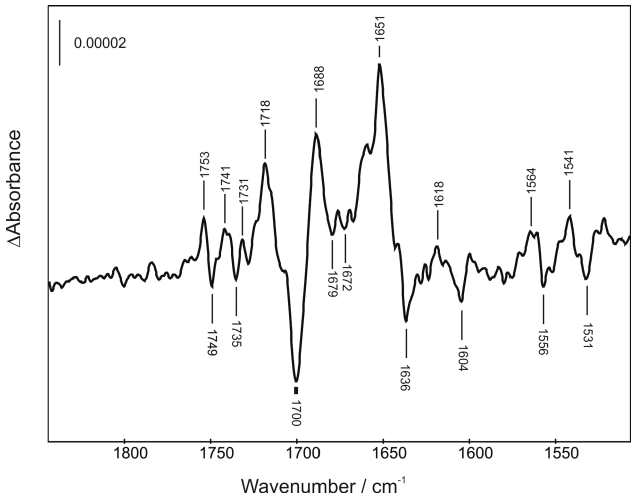

Figure 8. Light-induced difference spectra of PS I immobilized by a His-tag on the generated silane-SAM. The spectrum shows changes in the hydrogen bonds of the chlorophyll molecule.[30]

of the earlier studies suffer from less stable attachment, but the introduction of a hydrophilic barrier led to stable attachment.[22] However, so far, fairly drastic reaction conditions or incompatible solvents or irradiation procedures had to be used that prevent in situ SAM formation.[14,32,33] The SAM formation in a flow through cuvette within the spectrometer achieved in our approach allows for a direct quality control and simple applicability. We further optimized hydroxylation conditions to avoid the generation of a thick signal-decreasing oxide layer on the germanium crystal, which was caused by HNO_3 treatment.[22] In particular, the edge of incidence into the IRE is not affected by peroxide/oxalic acid treatment, leading to better signal-to-noise ratio. Further, in contrast to other immobilization techniques in which either undecane[34] or CCl_4[22] are used, the use of 2-propanol as solvent allows fast and complete exchange to the aqueous environment in the flowthrough system.

In particular, the native immobilization of transmembrane proteins is of broad interest. The available techniques have been recently reviewed.[1] In contrast to our method, most of the described techniques do not generate the high surface concentrations needed for ATR-FTIR difference spectroscopy. One of the techniques established for FTIR is surface-enhanced infrared absorption (SEIRA). Here, the protein is attached to a functionalized thiol-SAM build up on a heterogeneous gold island layer.[11] On one hand, the island structure of the gold layer is responsible for signal enhancement; on the other hand, the gold layer largely absorbs in the infrared. This leads to a drastic signal decrease, so that only single-reflection ATR crystals can be used. The missing enhancement effect of germanium IREs can easily be compensated by using multiple internal reflections, leading to comparable signal-to-noise ratio. The SEIRA technique is especially useful if a metal layer is necessary for the investigation of electrochemically active proteins. However, the SEIRA spectrum cannot give information on the orientation, as the electric field components parallel to the surface are completely absorbed by the gold layer. A further big advantage of using germanium is the much broader spectral window (Figure S10, Supporting Information) down to 830 cm^{-1}, compared to silicon (>1470 cm^{-1}).

CONCLUSION

In this work, we have demonstrated convenient and efficient surface functionalization of germanium for the immobilization of His-tagged proteins. Besides the ATR-FTIR spectroscopy, we used X-ray-photoelectron spectroscopy to characterize the chemically modified germanium. In three steps, we generated a histidine affinity surface that can be used for the immobilization of any His-tagged protein. In the first step, the germanium crystal was activated, leading to a hydroxylated surface. Second, the mixture of linker−silane and matrix−silane was attached to the surface in situ. In the last preparation step, the terminal succinimidyl ester reacted with ANTA. In the presence of nickel, His-tagged proteins were specifically immobilized and remained functional, as shown by ATR-FTIR difference spectroscopy. The small GTPase Ras was attached via His-tag, and its function as a molecular switch was shown in a beryllium trifluoride anion titration assay. High specificity was proven by the repeated association and dissociation with imidazole. His-tagged PS I was immobilized in detergent and showed light-induced activity. The orientation of the attached PS I was studied by polarized ATR-FTIR-difference spectroscopy. Immobilized PS I and N-Ras showed activity for at least 1 day. The described regeneration of the surface makes repeated measurements like the analysis of different substrates or drugs extremely convenient.

We show the first stimulus-induced difference spectra of monolayered proteins attached via silanization chemistry without surface-enhanced effect. Our technique provides the opportunity to analyze His-tagged proteins at atomic resolution. This will be an excellent tool in the very important field of the study of pharmaceutically relevant proteins like Ras or GPCRs and their interaction with drugs.

ASSOCIATED CONTENT

Supporting Information

Calculation of protein surface concentrations; surface concentrations of immobilized Ras and PS I molecules; Figure S1, difference spectrum of the attachment of linker−silane on germanium; Figure S2, molar ratio of linker−silane and matrix−silane; Figure S3, XPS region scans of a germanium crystal modified with silanes; Figure S4, comparison of the amide I and II regions of N-Ras bound to NTA−lipids or NTA−silanes; Figure S5, binding kinetics of N-Ras with the decahistidine-tag on a modified germanium surface with different linker concentrations; Figure S6, detachment of N-Ras with different concentrations of imidazole; Figure S7, determination of the EC_{50} value by using different imidazole concentrations for the detachment of N-Ras; Figure S8, comparison of BeF_3^--induced difference spectra of N-Ras bound via a semisynthetic anchor to POPC-lipids or via His-tag to NTA−silanes; Figure S9, comparison of amide I and amide II from N-Ras and PS I; Figure S10, comparison of the single channel spectra of germanium with silicon; Figures S11−S16, ^1H and ^{13}C NMR spectra of synthesized compounds. This material is available free of charge via the Internet at http://pubs.acs.org.

AUTHOR INFORMATION

Corresponding Author

carsten.koetting@rub.de

Notes

The authors declare no competing financial interest.

■ ACKNOWLEDGMENTS

We thank Philipp Pinkerneil for preparation of decahistidine-tagged N-Ras1−180, Sarah Jenrich for the preparation of H-Ras1−166, and Marta Kopczak for purified photosystem I. We are grateful for the financial support by the Deutsche Forschungsgemeinschaft (SFB 642) and the CVM (cofinanced by the EU and the state North Rhine-Westphalia). Support by the Federal Ministry of Education and Research (BMBF, project H_2 design cells; M.R.) is gratefully acknowledged.

■ REFERENCES

(1) Früh, V.; IJzerman, A. P.; Siegal, G. *Chem. Rev.* **2011**, *111*, 640−656.
(2) Badura, A.; Esper, B.; Ataka, K.; Grunwald, C.; Wöll, C.; Kuhlmann, J.; Heberle, J.; Rögner, M. *Photochem. Photobiol.* **2006**, *82*, 1385−1390.
(3) Lata, S.; Piehler, J. *Nat. Protoc.* **2006**, *1*, 2104−2109.
(4) Maalouli, N.; Gouget-Laemmel, A. C.; Pinchemel, B.; Bouazaoui, M.; Chazalviel, J.-N.; Ozanam, F.; Yang, Y.; Burkhard, P.; Boukherroub, R.; Szunerits, S. *Langmuir* **2011**, *27*, 5498−5505.
(5) Waichman, S.; You, C.; Beutel, O.; Bhagawati, M.; Piehler, J. *Anal. Chem.* **2011**, *83*, 501−508.
(6) Waichman, S.; Bhagawati, M.; Podoplelova, Y.; Reichel, A.; Brunk, A.; Paterok, D.; Piehler, J. *Anal. Chem.* **2010**, *82*, 1478−1485.
(7) Knezevic, J.; Langer, A.; Hampel, P. A.; Kaiser, W.; Strasser, R.; Rant, U. *J. Am. Chem. Soc.* **2012**, *134*, 15225−15228.
(8) Willander, M.; Al-Hilli, S. *Methods Mol. Biol.* **2009**, *544*, 201−229.
(9) Kötting, C.; Gerwert, K. *ChemPhysChem* **2005**, *6*, 881−888.
(10) Vigano, C.; Ruysschaert, J.-M.; Goormaghtigh, E. *Talanta* **2005**, *65*, 1132−1142.
(11) Ataka, K.; Kottke, T.; Heberle, J. *Angew. Chem., Int. Ed.* **2010**, *49*, 5416−5424.
(12) Kötting, C.; Güldenhaupt, J.; Gerwert, K. *Chem. Phys.* **2012**, *396*, 72−83.
(13) Pinkerneil, P.; Güldenhaupt, J.; Gerwert, K.; Kötting, C. *ChemPhysChem* **2012**, *13*, 2649−2653.
(14) Devouge, S.; Salvagnini, C.; Marchand-Brynaert, J. *Bioorg. Med. Chem. Lett.* **2005**, *15*, 3252−3256.
(15) Goormaghtigh, E.; Raussens, V.; Ruysschaert, J. M. *Biochim. Biophys. Acta* **1999**, *1422*, 105−185.
(16) Cox, A. D.; Der, C. J. *Small GTPases* **2010**, *1*, 2−27.
(17) Golbeck, J. H. *Annu. Rev. Plant Physiol. Plant Mol. Biol.* **1992**, *43*, 293−324.
(18) Chitnis, P. R. *Annu. Rev. Plant Physiol. Plant Mol. Biol.* **2001**, *52*, 593−626.
(19) Tucker, J.; Sczakiel, G.; Feuerstein, J.; John, J.; Goody, R. S.; Wittinghofer, A. *EMBO J.* **1986**, *5*, 1351−1358.
(20) El-Mohsnawy, E.; Kopczak, M. J.; Schlodder, E.; Nowaczyk, M.; Meyer, H. E.; Warscheid, B.; Karapetyan, N. V.; Rögner, M. *Biochemistry* **2010**, *49*, 4740−4751.
(21) Güldenhaupt, J.; Rudack, T.; Bachler, P.; Mann, D.; Triola, G.; Waldmann, H.; Kötting, C.; Gerwert, K. *Biophys. J.* **2012**, *103*, 1585−1593.
(22) Devouge, S.; Conti, J.; Goldsztein, A.; Gosselin, E.; Brans, A.; Voué, M.; De Coninck, J.; Homblé, F.; Goormaghtigh, E.; Marchand-Brynaert, J. *J. Colloid Interface Sci.* **2009**, *332*, 408−415.
(23) Ataka, K.; Giess, F.; Knoll, W.; Naumann, R.; Haber-Pohlmeier, S.; Richter, B.; Heberle, J. *J. Am. Chem. Soc.* **2004**, *126*, 16199−16206.
(24) Socrates, G. *Infrared and Raman Characteristic Group Frequencies: Tables and Charts*; John Wiley & Sons: West Sussex, UK, 2007, ISBN 0-470-09307-2.
(25) Prabhakaran, K.; Ogino, T. *Surf. Sci.* **1995**, *325*, 263−271.
(26) Yang, M.; Wouters, D.; Giesbers, M.; Schubert, U. S.; Zuilhof, H. *ACS Nano* **2009**, *3*, 2887−2900.
(27) Pai, E. F.; Kabsch, W.; Krengel, U.; Holmes, K. C.; John, J.; Wittinghofer, A. *Nature* **1989**, *341*, 209−214.
(28) Lata, S.; Piehler, J. *Anal. Chem.* **2005**, *77*, 1096−1105.
(29) Kötting, C.; Kallenbach, A.; Suveyzdis, Y.; Eichholz, C.; Gerwert, K. *ChemBioChem* **2007**, *8*, 781−787.
(30) Iwaki, M.; Andrianambinintsoa, S.; Rich, P.; Breton, J. *Spectrochim. Acta A Mol. Biomol. Spectrosc.* **2002**, *58*, 1523−1533.
(31) Rigler, P.; Ulrich, W.-P.; Hoffmann, P.; Mayer, M.; Vogel, H. *ChemPhysChem* **2003**, *4*, 268−275.
(32) Matijasević, J.; Hassler, N.; Reiter, G.; Fringeli, U. P. *Langmuir* **2008**, *24*, 2588−2596.
(33) Smith, B. M.; Lappi, S. E.; Brewer, S. H.; Dembowy, S.; Belyea, J.; Franzen, S. *Langmuir* **2004**, *20*, 1184−1188.
(34) Zhang, S.; Koberstein, J. T. *Langmuir* **2012**, *28*, 486−493.